Earthquakes and Structures, *Vol. 15, No. 3 (2018) 243-251*
DOI: https://doi.org/10.12989/eas.2018.15.3.243

Dynamic response of post-tensioned rocking wall-moment frames under near-fault ground excitation

Ruoyu Feng[1a], Ying Chen[*2] and Guozhi Cui[2]

[1]*School of Aerospace Engineering, Tsinghua Univerisity, Beijing, China*
[2]*School of Civil Engineering, Shandong University, Jinan, China*

(Received January 21, 2018, Revised April 27, 2018, Accepted June 3, 2018)

Abstract. The dynamic responses of a rocking wall-moment frame (RWMF) with a post-tensioned cable are investigated. The nonlinear equations of motions are developed, which can be categorized as a single-degree-of-freedom (SDOF) model. The model is validated through comparison of the rocking response of the rigid rocking wall (RRW) and displacement of the moment frame (MF) against that obtained from Finite Element analysis when subjected ground motion excitation. A comprehensive parametric analysis is carried out to determine the seismic performance factors of the RWMF systems under near-fault trigonometric pulse excitation. The horizontal displacement of the RWMF system is compared with that of MF structures without RRW, revealing the damping effect of the RRW. Frame displacement spectra excited by trigonometric pulses and recorded earthquake ground motions are constructed. The effects of pulse type, mass ratio, frame stiffness, and wall slenderness variations on the displacement spectra are presented. The paper shows that the coupling with a RRW has mixed results on suppressing the maximum displacement response of the frame.

Keywords: rocking wall-moment frame; post-tension; rocking wall; damping; spectra; earthquake; near-fault

1. Introduction

In recent years, the need to improve the seismic performance of buildings has led to the development of innovative systems such as rocking wall-moment frame (RWMF) combinations (Makris 2014). The rigid rocking wall (RRW) is restrained by the moment frame (MF) and allowed to pivot about its base. The function of the wall is to provide additional damping, impose uniform drift along the height of the frame and reduce drift concentration (Qu *et al*. 2014).

The dynamic responses of a rocking block have been studied extensively (Housner 1963, Aslam *et al*. 1980, Makris *et al*. 2000). The idea of combining rocking walls and moment frames as enhanced earthquake resisting systems was introduced by Ajrab (2000). The actual implementation of an RWMF with supplementary energy dissipation devices was reported in recent years (Ajrab *et al*. 2014, Wada *et al*. 2011, Grigorian *et al*. 2015, Qu *et al*. 2014, Loo *et al*. 2015). Qu *et al*. (2014) adopted a pinned rocking wall with dampers for controlling the deformation pattern of an 11-story ductile frame structure. Nevertheless, Makris (2017) pointed out that the concept of the pinned wall should be used with caution since the pinned wall amplifies the response for most of the range of the spectrum.

The majority of existing literature emphasize on the inelastic behavior and capacity design of RWMF systems, without analyzing its dynamic response theoretically. Thus, in this paper, the dynamic perspective of a practical RWMF system with a post-tension cable under near-fault ground excitation is investigated, the nonlinear equations of motions are derived, and the influence of a rocking wall on the responses of the coupled system is examined.

2. Dynamics of a RWMF system

2.1 Analytical model

A moment resisting frame coupled with a rocking wall can be categorized as a SDOF system, with the first-mode dominating its dynamic response. Accordingly, the MF is also idealized as a SDOF with a lumped mass m_s, lumped stiffness k_s and a viscous damping c_s, as illustrated in Fig. 1. The RRW can oscillate around the centers of rotation O and O'. The wall has a size of $R=\sqrt{h^2+b^2}$, slenderness $\alpha=a\tan(b/h)$, mass m_w and moment of inertia about the pivoting points O and O', $I_0=\frac{4}{3}m_wR^2$. The weight of the rocking wall is lumped at the centroid of the wall. The coefficient of friction is large enough so that sliding does not occur between the pivot point and the wall base.

The RRW is placed on top of a rigid foundation. The wall is pin-jointed to the frame at roof level with an arm length of L. A post-tension cable is placed along the vertical line passing through the centroid of the wall. The cable is unbonded to the surrounding wall material so that it can

∗Corresponding author, Professor
E-mail: chenying@sdu.edu.cn
[a]Ph.D. Student
E-mail: fry18@mails.tsinghua.edu.cn

ISSN: 2092-7614 (Print), 2092-7622 (Online)

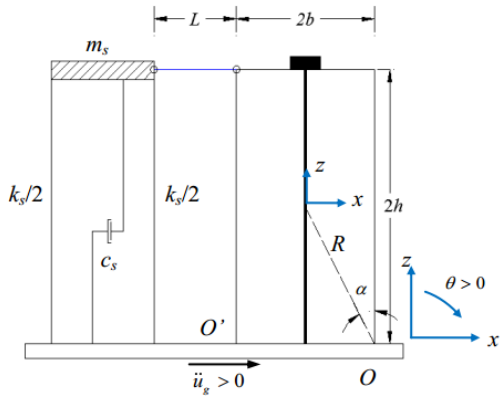

Fig. 1 A rocking wall-moment frame

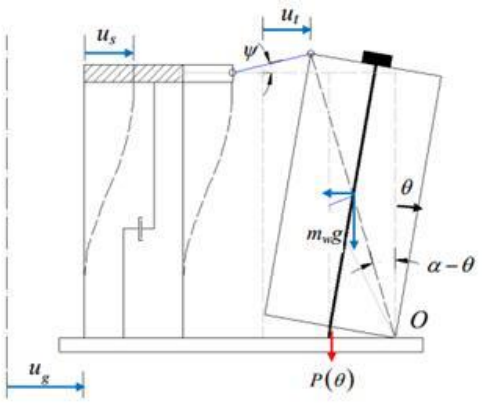

(a) Positive rotation

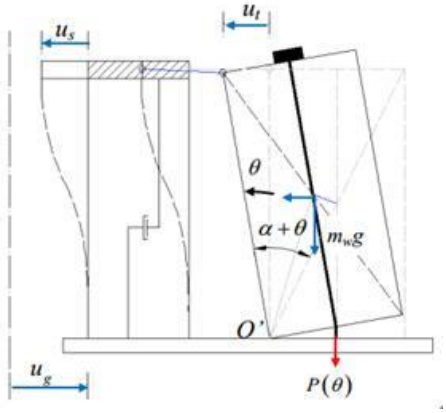

(b) Negative rotation

Fig. 2 A RWMF system under ground motion

deform freely.

Under a positive horizontal ground acceleration $\ddot{u}_g$ (the ground is accelerating to the right), the MF will sway to the left and the RRW will initially rock to the left (rotation about point O') with a negative rotation, $\theta<0$, as shown in Fig. 2(b), and it will eventually assume a positive rotation with the MF swaying to right, as shown in Fig. 2(a).

The post-tension force can be represented by two dimensionless parameters, η_0 and η_α. If $P(\theta=0)=\eta_0 m_w g$ and $P(\theta=\alpha)=\eta_\alpha m_w g$, then

$$P(\theta)=m_w g\left[\eta_0+(\eta_\alpha-\eta_0)\frac{\theta}{\alpha}\right] \tag{1}$$

During rocking motion, the center of mass of the RRW uplifts by v_w, the left top corner uplifts by v_t, and $v_t=2v_w$. The horizontal translation of the centroid of the wall is u_w, the horizontal displacement of the left top corner is u_t, and $u_t=2u_w$.

Assuming that the roof diaphragm is rigid and the motion of the MF is only a translation. The initially horizontal coupling link rotates by an angle ψ, which is related to the horizontal displacement of the MF mass, u_s, via the expression

$$\cos\psi=1+\frac{u_t-u_s}{L}\qquad \sin\psi=\frac{v_t}{L} \tag{2}$$

Considering $\cos\psi^2+\sin\psi^2=1$, the following expression holds

$$\frac{u_s}{L}=1+\frac{u_t}{L}-\sqrt{1-\left(\frac{v_t}{L}\right)^2} \tag{3}$$

Assuming that the coupling arm is long enough, $(u_t/L)^2<<1$, then $u_s=u_t=2u_w$.

The MF mass displacement u_s and its derivatives with respect to time for $\theta(t)<0$ and $\theta(t)>0$ are given by

$$u_s=\pm 2R\left[\sin\alpha\mp\sin(\pm\alpha-\theta)\right] \tag{4}$$

$$\dot{u}_s=2R\dot{\theta}\cos(\pm\alpha-\theta) \tag{5}$$

$$\ddot{u}_s=2R\left[\ddot{\theta}\cos(\pm\alpha-\theta)+\dot{\theta}^2\sin(\pm\alpha-\theta)\right] \tag{6}$$

whenever there is a double sign (say ±) the top sign is for $\theta>0$ and the bottom sign is for $\theta<0$.

Case 1: $\theta>0$

The balance of angular moment with respect to O leads to Eq. (7)

$$\begin{gathered}\frac{4}{3}m_w R^2\ddot{\theta}+2R\cos(\alpha-\theta)\left[m_s\left(\ddot{u}_s+\ddot{u}_g\right)+k_s u_s+c_s\dot{u}_s\right]=\\ -m_w R\left[\ddot{u}_g\cos(\alpha-\theta)+g\sin(\alpha-\theta)\right]-P(\theta)R\sin\alpha\\ \text{for}\quad \theta>0\end{gathered} \tag{7}$$

Substituting Eqs. (1), (4) to (6) into Eq. (7), defining $\gamma=m_s/m_w$ the mass ratio, $\omega_s=\sqrt{k_s/m_s}$ the undamped frequency and $\xi_s=\dfrac{c_s}{2m_s\omega_s}$ the viscous damping ratio of the SDOF MF, and after suitable mathematical manipulations, we obtain

$$\begin{gathered}\left[\frac{4}{3}+4\gamma\cos^2(\alpha-\theta)\right]\ddot{\theta}=-4\gamma\cos(\alpha-\theta)\\ \sin(\alpha-\theta)\dot{\theta}^2-8\gamma\cos^2(\alpha-\theta)\omega_s\xi_s\dot{\theta}\\ -\frac{(2\gamma+1)}{R}\cos(\alpha-\theta)\ddot{u}_g-4\gamma\cos(\alpha-\theta)\omega_s^2\left[\sin\alpha-\sin(\alpha-\theta)\right]\\ -\frac{1}{R}g\sin(\alpha-\theta)-\frac{g}{R}\left[\eta_0+(\eta_\alpha-\eta_0)\frac{\theta}{\alpha}\right]\sin\alpha\end{gathered} \tag{8}$$

Case 2: $\theta<0$

For negative rotations, the balance of angular moment with respect to O' leads to Eq. (9)

$$\frac{4}{3}m_w R^2\ddot{\theta}+2R\cos\alpha\cos\theta\left[m_s\left(\ddot{u}_s+\ddot{u}_g\right)+k_s u_s+c_s\dot{u}_s\right]=$$
$$-m_w R\left[\ddot{u}_g\cos\left(-\alpha-\theta\right)+g\sin\left(-\alpha-\theta\right)\right]+P\left(\theta\right)R\sin\alpha \quad (9)$$
$$\text{for}\quad \theta<0$$

The equation of motion of the coupled system for θ<0 is

$$\left[\frac{4}{3}+4\cos\alpha\cos\theta\gamma\cos\left(-\alpha-\theta\right)\right]\ddot{\theta}+4\gamma\cos\alpha\cos\theta\left(\sin\left(-\alpha-\theta\right)\dot{\theta}^2\right.$$
$$+2\omega_s\xi_s\cos\left(-\alpha-\theta\right)\dot{\theta}-\omega_s^2\left[\sin\left(-\alpha-\theta\right)+\sin\alpha\right]\Big)=$$
$$-\frac{1}{R}\left[2\cos\alpha\cos\theta\gamma+\cos\left(-\alpha-\theta\right)\right]\ddot{u}_g \quad (10)$$
$$-\frac{1}{R}g\sin\left(-\alpha-\theta\right)+\frac{g}{R}\left[\eta_0+\left(\eta_\alpha-\eta_0\right)\frac{\theta}{\alpha}\right]\sin\alpha$$
$$\text{for}\quad \theta<0$$

When the frame is absent ($\gamma=\omega_s=\xi_s=0$), Eqs. (8) and (10) reduce to the equation of motion of a rocking block restrained with an unbonded post-tensioning cable (Barthe 2012)

$$I_0\ddot{\theta}=-m_w\ddot{u}_g R\cos\left(\alpha-\theta\right)-m_w gR\sin\left(\alpha-\theta\right)-P\left(\theta\right)R\sin\alpha \quad (11a)$$
$$\text{for}\quad \theta>0$$

$$I_0\ddot{\theta}=-m_w\ddot{u}_g R\cos\left(-\alpha-\theta\right)$$
$$-m_w gR\sin\left(-\alpha-\theta\right)+P\left(\theta\right)R\sin\alpha\quad\text{for}\quad\theta<0 \quad (11b)$$

Furthermore, when the post-tensioning cable is absent, $P(\theta)$=0, Eqs. (8) and (10) reduce to the equation of motion of the free-standing rocking block (Zhang *et al*. 2000)

$$I_0\ddot{\theta}=-m_w\ddot{u}_g R\cos\left(\alpha-\theta\right)-m_w gR\sin\left(\alpha-\theta\right) \quad (12a)$$
$$\text{for}\quad \theta>0$$

$$I_0\ddot{\theta}=-m_w\ddot{u}_g R\cos\left(-\alpha-\theta\right)-m_w gR\sin\left(-\alpha-\theta\right)\text{for}\quad\theta<0 \quad (12b)$$

The equations of motion, Eqs. (8) and (10), are valid for nonzero values of the rocking rotation ($\theta\neq0$).

2.2 State-space formulation

The dynamic response of the RWMF system subjected to ground motion excitation is computed numerically via a state-space formulation which can accommodate the non-linear nature of the problem

$$\left\{y\left(t\right)\right\}=\begin{Bmatrix}\theta\left(t\right)\\ \dot{\theta}\left(t\right)\end{Bmatrix} \quad (13)$$

and the time-derivative vector, $y(t)$, is

$$\left\{\dot{y}\left(t\right)\right\}=\begin{Bmatrix}\dot{\theta}\left(t\right)\\ \ddot{\theta}\left(t\right)\end{Bmatrix} \quad (14)$$

Eqs. (8) and (10) can be expressed in the compact form

$$\ddot{\theta}=\mathrm{A}_1\dot{\theta}^2+A_2\dot{\theta}+A_3\ddot{u}_g\left(t\right)+A_4 \quad (15a)$$
$$\text{for}\quad \theta<0$$

$$\ddot{\theta}=B_1\dot{\theta}^2+B_2\dot{\theta}+B_3\ddot{u}_g\left(t\right)+B_4\quad\text{for}\quad\theta>0 \quad (15b)$$

where,

$$\mathrm{A}_1=a_1a_2a_6;\quad A_2=a_1a_2a_5;\quad A_3=a_1a_3;$$
$$A_4=a_1a_2a_7-\frac{g}{R}a_1\left(a_6-a_4\right);$$
$$a_1=\frac{1}{\left[\frac{4}{3}+4\gamma\cos\alpha\cos\theta\cos\left(-\alpha-\theta\right)\right]};$$
$$a_2=-4\gamma\cos\alpha\cos\theta;$$
$$a_3=-\frac{1}{R}\left[2\gamma\cos\alpha\cos\theta+\cos\left(-\alpha-\theta\right)\right];$$
$$a_4=\left(\eta_0+\left(\eta_\alpha-\eta_0\right)\frac{\theta}{\alpha}\right)\sin\alpha;\quad a_5=2\omega_s\xi_s\cos\left(-\alpha-\theta\right)$$
$$;\quad \mathrm{a}_6=\sin\left(-\alpha-\theta\right);\quad a_7=-\omega_s^2\left[\sin\left(-\alpha-\theta\right)+\sin\alpha\right];$$
$$B_1=b_1b_2;\quad B_2=b_1b_3;\quad B_3=b_1b_4;\quad B_4=b_1b_5-\frac{g}{R}b_1a_4$$
$$b_1=\frac{1}{\left[\frac{4}{3}+4\gamma\cos^2\left(\alpha-\theta\right)\right]};$$
$$b_2=-4\gamma\cos\left(\alpha-\theta\right)\sin\left(\alpha-\theta\right);\quad b_3=-8\gamma\omega_s\xi_s\cos^2\left(\alpha-\theta\right);$$
$$b_4=-\frac{\left(2\gamma+1\right)}{R}\cos\left(\alpha-\theta\right);$$
$$b_5=-4\gamma\cos\left(\alpha-\theta\right)\omega_s^2\left[\sin\alpha-\sin\left(\alpha-\theta\right)\right]-\frac{g}{R}\sin\left(\alpha-\theta\right)$$

The differential equations are solved numerically in MATLAB adopting the ODE45 solver, which uses the 4th-5th order Runge-Kutta integration technique.

Energy dissipation occurs during impact and can be calculated by the ratio of kinetic energy before and after the impact, $r=\left(\dot{\theta}_2/\dot{\theta}_1\right)^2$. Damping effects due to wall rocking are included in numerical analysis by considering the restitution coefficient. At each impact (θ=0), the velocity at the previous step is automatically decreased by a factor equal to the restitution coefficient $\sqrt{r}=\dot{\theta}_2/\dot{\theta}_1$, and the boundary condition $y(t_e)$ is updated accordingly. The reduction of the velocity numerically occurs by means of an event-identification function, which stops the integration when the condition θ=0 has been attained at time t_e.

Experimental tests have been performed to identify the values of the restitution coefficients for specimens of various material and slenderness ratios (Sorrentino *et al*. 2011, Costa 2012), which depends on many parameters including the interface material, plastic deformations at the pivot points, and imperfections of the contact surface (Prieto *et al*. 2004). By recognizing the difficulty in correlating with the maximum rotation before impact or with the theoretical value, an average restitution coefficient of 0.9 is assumed in the following analyses.

3. Finite element validation

A three-dimensional Finite Element (FE) model is developed to validate the proposed model. The frame is

Table 1 Dynamic parameters of the RWMF system

b (m)	h (m)	α	γ	k_s (N/m)	ξ_s	m_w (N/g)	K_P (N/m)
0.5	2	0.2450	1800	7.2E+008	0.05	1600	143256

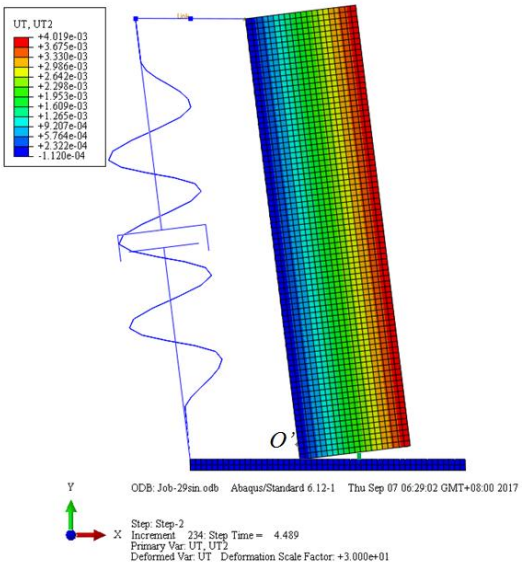

Fig. 3 Vertical displacement (m) of the FE model for a RWMF system

idealized as a SDOF mass-spring-dashpot model. A MASS element is attached to the parallel Spring2 and Dashpot2 elements, and the spring and dashpot are connected to the foundation with a dimension of 2.5×0.5×0.2 m. The connection between the frame and the wall is modeled using a connector element CONN3D2 which provides a pinned rigid link.

Only linear elastic material model is employed. A Poisson's ratio of 0.2 is adopted for all materials. An elastic modulus value of 30 GPa is used for the concrete wall, while a value of 300 GPa is assumed for the rigid foundation.

The connection between the wall and the foundation is modeled using a "surface to surface contact" interaction, with tangential behavior type "penalty" and normal behavior type "hard contact" under compressive stress. A friction coefficient of 0.35 is taken to simulate the tangential behavior.

Truss elements are used to model the cable, which has a pinned connection to the ground and is rigidly connected to the top of the wall by means of the "beam" type multi-point constrain.

A mesh composed of 8-node linear brick elements and reduced integration is used both for the wall and the foundation. The maximum element size is 50 mm. The U_1, U_2 and UR_3 degrees of freedom of all the wall nodes are constrained to the rigid body motion of the centroid of the wall by a kinematic coupling definition.

For the model being studied, the dynamic parameters are presented in Table 1.

Three loading steps are created: in the first load step the boundary conditions are set and the weight of the wall is applied at its centroid; in the second load step the

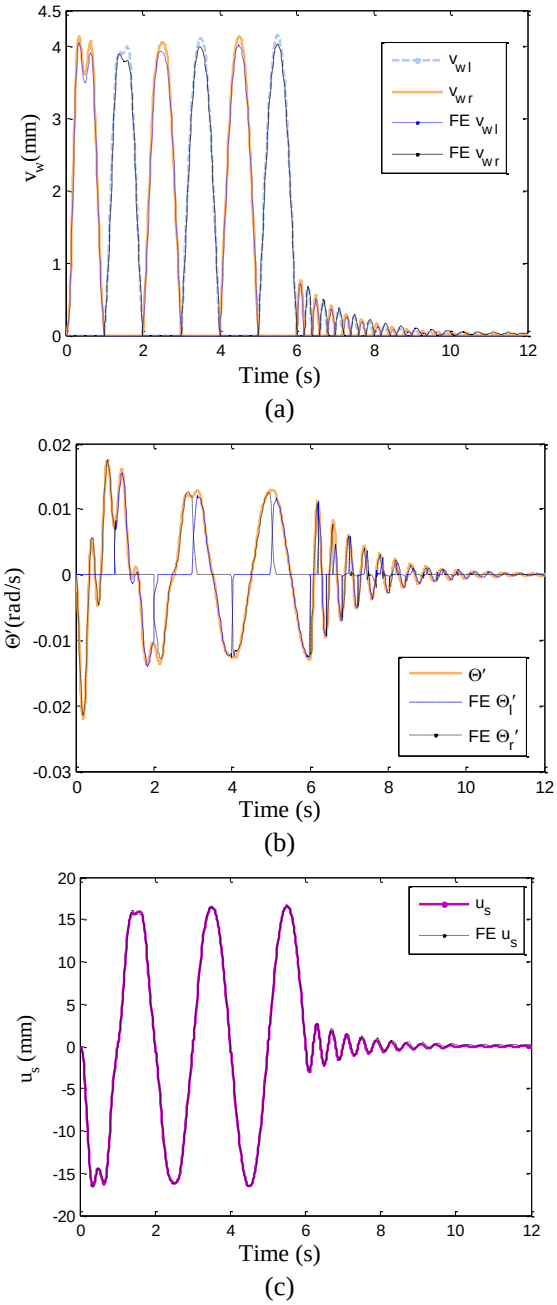

Fig. 4 Comparison of the wall left corner uplift v_{wl} (a), wall right corner uplift v_{wr} and angular velocity $\dot{\theta}$ (b), displacement u_s (c) response of a RWMF (T_s=0.4 s, γ=1800, ξ_s=0.05, tan α=0.5/2) from the proposed model and FE analysis

prestressing force is applied to the cable; in the third load step the nonlinear dynamic analysis is performed, and the model is subjected to a four-cycle sinusoidal pulse excitation with an amplitude of 0.4 g, angular frequency of ω_p=2π and duration of 6 s.

Fig. 3 shows the vertical deformation of the FE model of the RWMF system in meter.

The response obtained by numerical solution of the proposed RWMF model, in terms of the left corner uplift u_{wl}, right corner uplift u_{wr}, angular velocity $\dot{\theta}$ of the RRW,

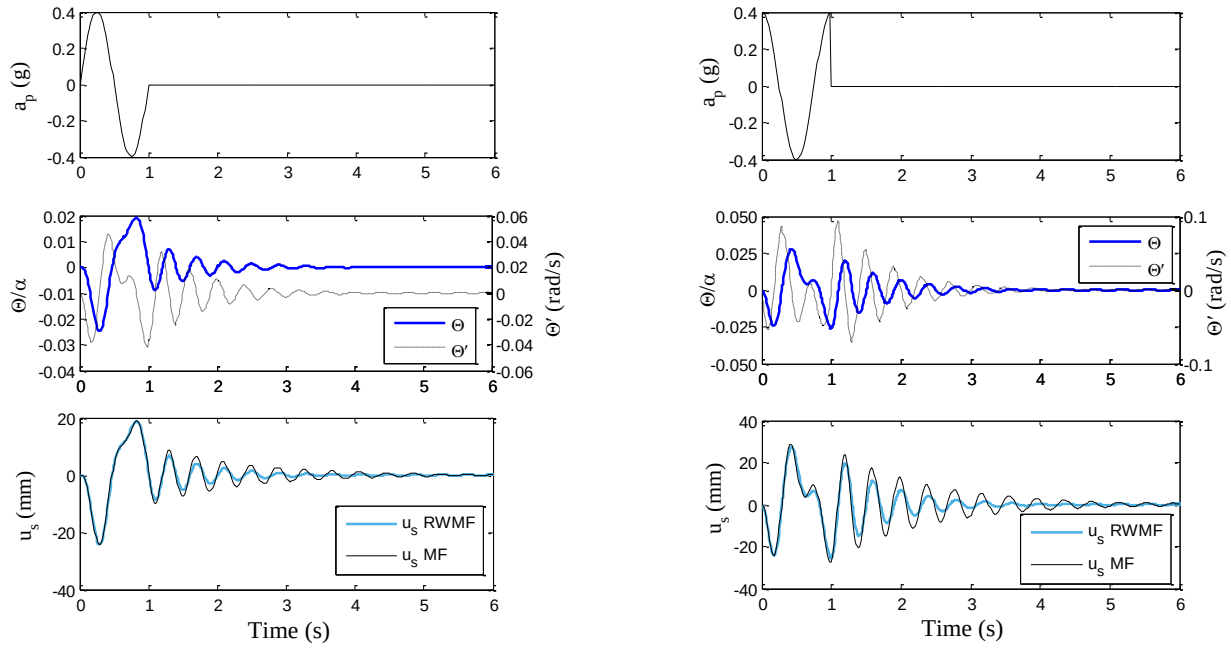

(a) One-sine pulse (b) One-cosine pulse

Fig. 5 Response of RWMF (T_s=0.4 s, γ=1800, ξ_s=0.05, tanα=0.5/2) and corresponding MF structure subjected to a one-sine (a) and a one-cosine (b) pulse excitation

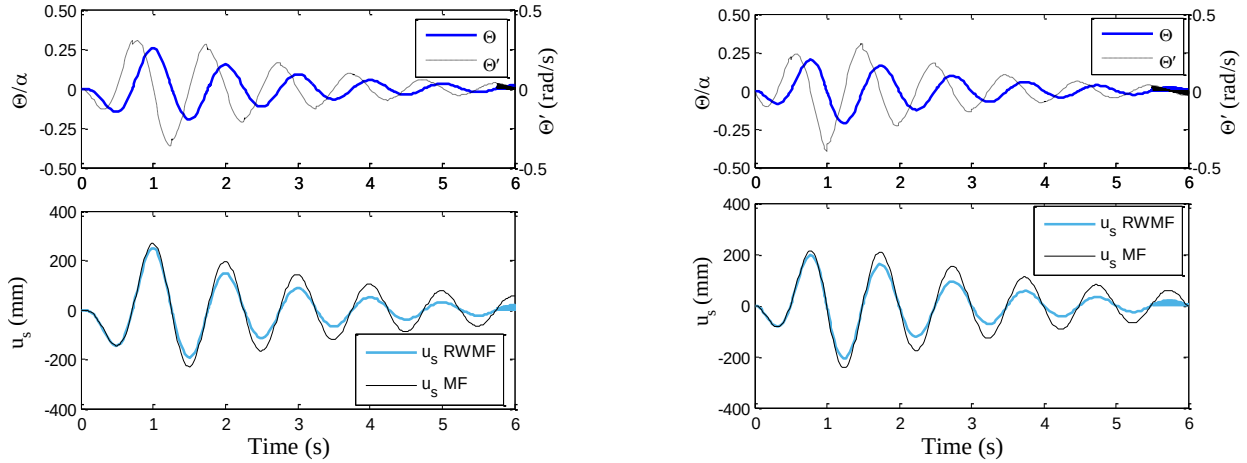

(a) One-sine pulse (b) One-cosine pulse

Fig. 6 Response of RWMF (T_s=1 s, γ=1800, ξ_s=0.05, tanα=0.5/2) and corresponding MF structure subjected to a one-sine (a) and a one-cosine (b) pulse excitation

and MF mass displacement u_s, are compared to that obtained from FE analysis under the same excitation, as shown in Fig. 4. The matches between the dynamic response produced by the FE and the proposed model are excellent. Eq. (15) can be considered as a global approximation of the time history of the RWMF system.

4. Response to near-fault trigonometric pulse excitation

Many recorded strong near-fault ground motions contain one or more relatively long-duration coherent pulses (Zhang *et al*. 2000). A simple pulse defined by few parameters (i.e., pulse type, pulse period T_p , and pulse intensity ($a_{g,max}$) can adequately describe the impulsive character of near-fault ground motions both qualitatively and quantitatively.

Forward (non-reversing) ground displacements can be described with a one-sine pulse (Makris 2015)

$$\ddot{u}_g(\tau) = \omega_p \frac{v_p}{2} \sin(\omega_p \tau), 0 \le \tau \le T_p \tag{16}$$

where τ=t−t_0, and t_0 is the time in the record when the trigonometric pulse initiates.

Some near-source ground motions result in a forward-and-back pulse, which can be captured with a one-cosine pulse

$$\ddot{u}_g(\tau) = \omega_p v_p \cos(\omega_p \tau), 0 \le \tau \le T_p \tag{17}$$

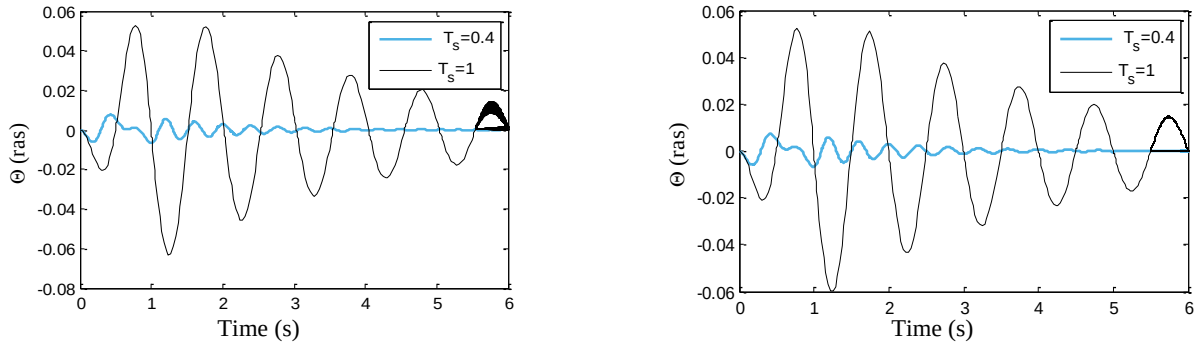

(a) γ=5 (b) γ=1800

Fig. 7 Wall rotation of RWMF (ξ_s=0.05, tanα=0.5/2) with different frame period under a one-cosine pulse excitation

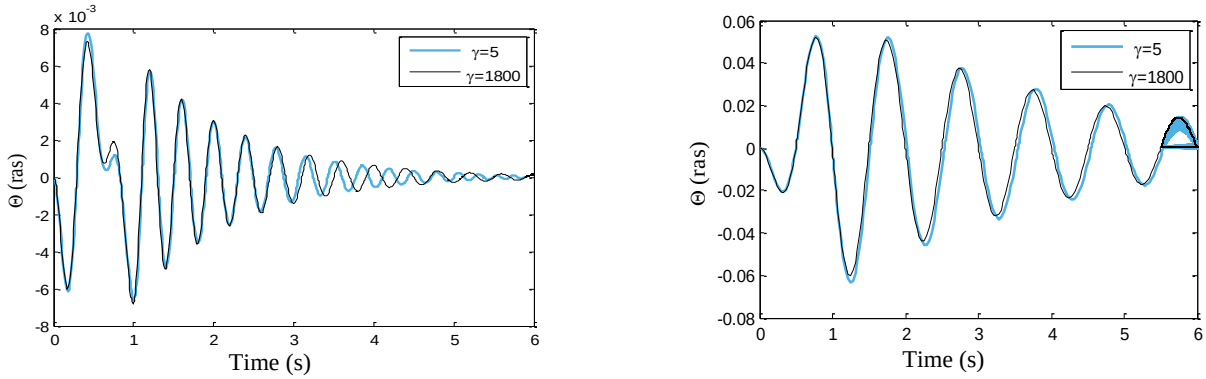

(a) T_s=0.4 s (b) T_s=1 s

Fig. 8 Wall rotation of RWMF (ξ_s=0.05, tanα=0.5/2) with different mass ratio under a one-cosine pulse excitation

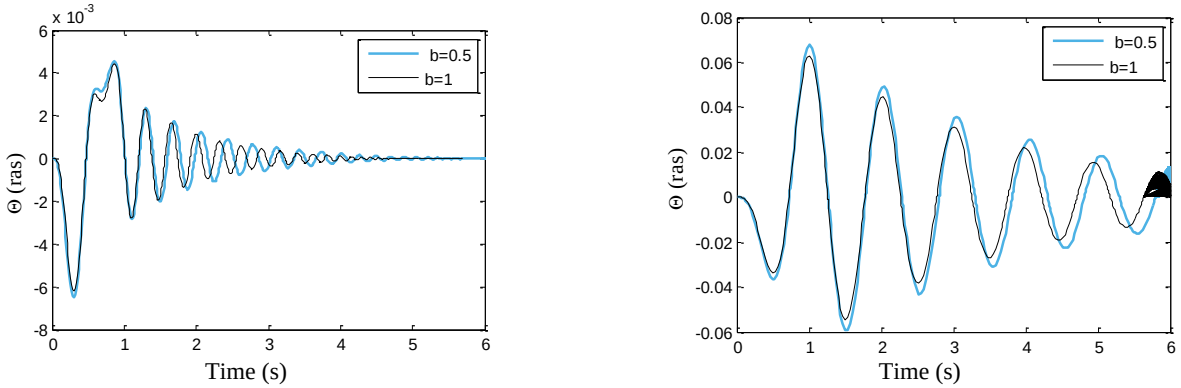

(a)T_s=0.4 s (b) T_s=1 s

Fig. 9 Rotation of the RRW of a RWMF (γ=5, ξ_s=0.05, h=2 m) with different rocking wall width under a one-cosine pulse excitation

In this section, the responses of a RWMF system subjected to a one-sine pulse or a one-cosine pulse excitation with amplitude of 0.4 g, angular frequency of $\omega_p=2\pi$ and duration of 1 s are investigated.

The second rows in Fig. 5 and Fig. 6 show the normalized rotation θ/α, angular velocity $\dot{\theta}$ of the wall of a RWMF system (γ=1800, ξ_s=0.05, tan α =0.5/2). For very stiff frame (T_s=0.4 s in Fig. 5), the maximum rotation and angular velocity caused by the sine pulse (left) are less than the maximum rotation under the cosine pulse excitation (right). While for a frame with mild stiffness (T_s=1 s in Fig. 6), the differences between the two maximum rotation and the two maximum angular velocities caused by two types of pulses are very small.

The last rows in Fig. 5 and Fig. 6 are the comparison of displacement u_s of a RWMF system with that of the same MF structure without rocking wall. The rocking wall demonstrates good energy dissipation ability under both types of pulse excitation, without suppressing the maximum displacement u_{smax}. For very stiff frame (T_s=0.4 s), u_{smax} caused by the sine pulse is less than that caused by the cosine pulse excitation. While for a frame with mild stiffness (T_s=1 s), u_{smax} caused by the sine pulse is larger than that caused by the cosine pulse.

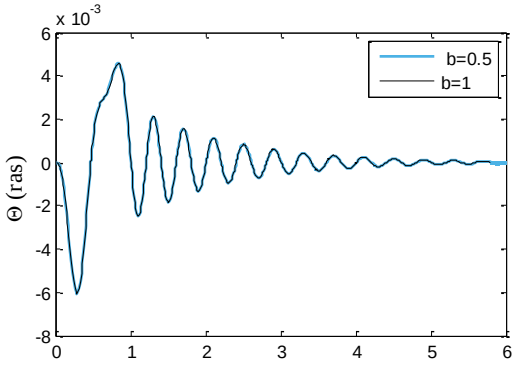

(a) T_s=0.4 s

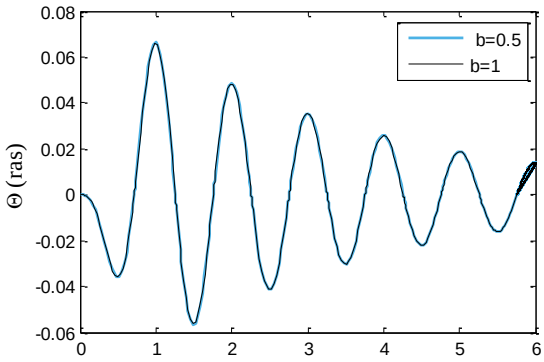

(b) T_s=1 s

Fig. 10 Rotation of the RRW for a RWMF (γ=1800, ξ_s=0.05, h=2 m) subjected to a one-cosine pulse excitation with different wall width

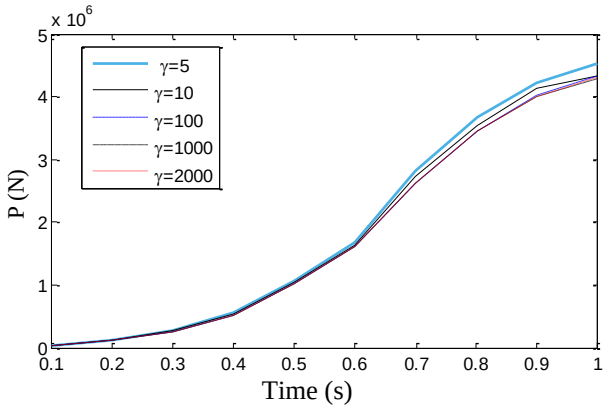

Fig. 11 Spring force of RWMF (ξ_s=0.05, tanα=0.5/2) subjected to a one-cosine pulse excitation for different frame period, T_s, and different mass ratio

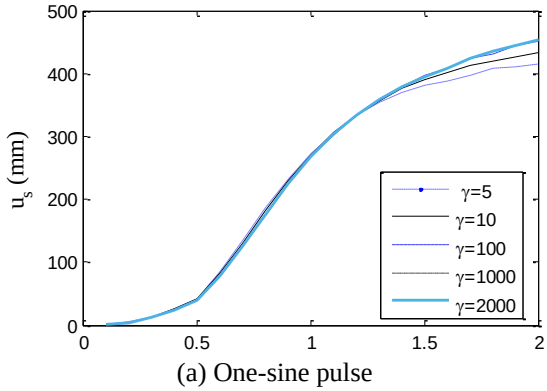

(a) One-sine pulse

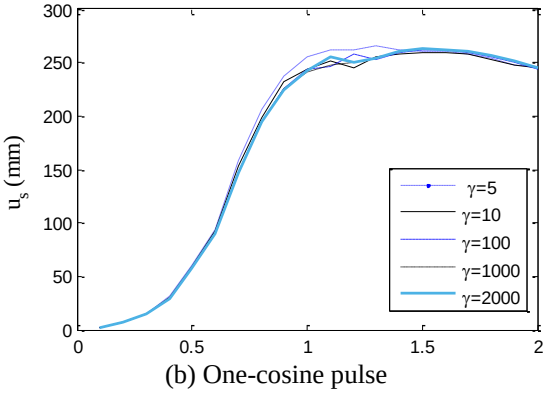

(b) One-cosine pulse

Fig. 12 Displacement spectra of a RWMF system (ξ_s=0.05, tanα=0.5/2) for five values mass ratio γ=5, 10, 100, 1000, 2000 when subjected to a one-sine (a) and a one-cosine (b) pulse excitation

Another major difference between the very stiff and the mild stiff frame cases is the rocking wall rotation. As observed in Fig. 7, under the one-cosine pulse excitation, a wall coupled with a frame of mild stiffness (T_s=1 s) oscillates less frequently but more strongly than that of a wall coupled with stiff frame (T_s=0.4 s). These oscillations can be so strong that they result in large frame displacement, as indicated in the last row of Fig. 6 (b).

Fig. 8 shows the comparison between rocking rotations of RWMF systems (ξ_s=0.05, tanα=0.5/2) with different mass ratio under the one-cosine pulse excitation. For both the very stiff frame (T_s=0.4 s) and the mild flexible frame (T_s=1 s) cases, the mass ratio has marginal influence on the rocking rotation of the wall.

The time histories of the rocking response of a 4 m tall RRW with b= 0.5 m and 1 m, respectively, to a one-cosine pulse excitation are plotted in Fig. 9 and Fig. 10.

When the mass ration is small such as γ=5, for a RWMF with a frame of mild stiffness (T_s=1 s), higher wall slenderness leads to larger rotation (Fig. 9(b)). Damping because of impact is strongly influenced by the slenderness: the squatter the wall is, the more energy it loses in every impact. For a RWMF with very stiff frame (T_s=0.4 s), the rotation responses of RWW are not sensitive to the wall slenderness parameter (Fig. 9(a)).

For large mass ratio γ=1800, the MF dominates the overall response the RWMF system, and the wall rotation has no dependence on the slenderness of the wall for both mild flexible frame (T_s=1 s) and very stiff frame (T_s=0.4 s) cases, as shown in Fig. 10.

Fig. 11 shows the maximum cable force increment of a RWMF (ξ_s=0.05, tanα=0.5/2) with a frame of different period T_s, and different mass ratio γ, when subjected to a one-cosine pulse excitation. The cable force increases as the frame period increases and provides stability against the overturning of the rocking wall.

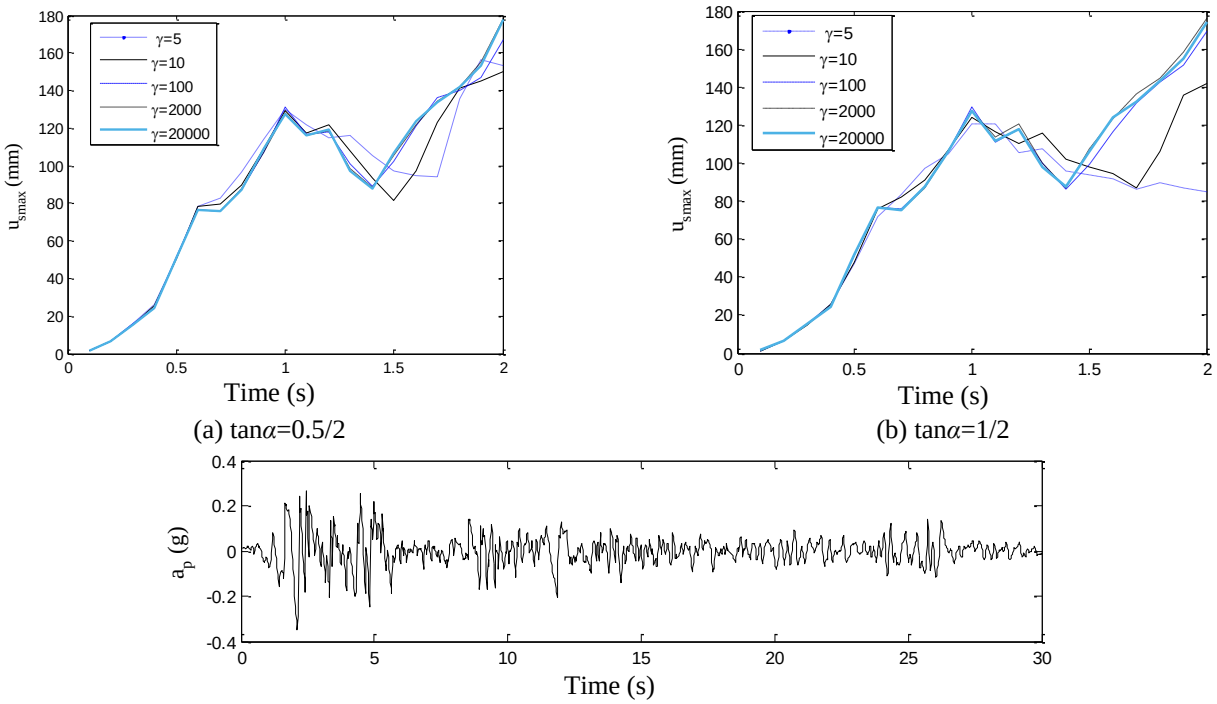

(a) tanα=0.5/2 (b) tanα=1/2

(c) Acceleration time history of the N-S Component of 1940 EL Centro earthquake

Fig. 13 Displacement spectra of a RWMF system (ξ_s=0.05, h = 2 m) for five values of mass ratio γ =5, 10, 100, 2000, 20000 and two values of wall slenderness, tanα=0.5/2 (a) and tanα=1/2 (b) when subjected to the North-South Component of 1940 EL Centro earthquake

5. Displacement spectra of a RWMF system

The equation of motions (15) is used to generate earthquake response spectra.

Fig. 12 displays the displacement spectra of a RWMF system (ξ_s=0.05, tanα=0.5/2 for values of mass ratio γ =5, 10, 100, 1000, 2000, when subjected to a one-sine (left) and a one-cosine (right) pulse excitation.

Fig. 12 reveals that, the RWMF subjected to a one-cosine pulse excitation exhibits lower maximum displacement responses, u_{smax}, than that of a RWMF subjected to a one-sine pulse excitation. For values of T_s≤1 s, the mass ratio appears to have marginal effect on u_{smax}. For values of T_s>1.4 s, the u_{smax} response of a RWMF with large mass ratio is larger than that of a RWMF with small mass ratio under the one-sine pulse excitation, while the difference in mass ratio has negligible effect on the u_{smax} response of the RWMF under the one-cosine pulse excitation.

Fig. 13 plots the displacement spectra of an RWMF for five values of mass ratio γ=5, 10, 100, 2000, 20000, and two values of wall slenderness, tanα=0.5/2 and tanα=1/2, when excited by the near fault north-south component of ground motion recorded at El Centro Terminal Substation during the 18 May 1940 Imperial Valley, California earthquake, as portrayed in Fig. 13 (c).

When observing Fig. 13, one can conclude that only the relative heavier wall, γ=5 or 10, could suppresses the u_{smax} response of very flexible frame (T_s>1.5 s). For frames with mild stiffness (T_s=0.6 s to 1.5 s), the presence of the rocking wall amplifies u_{smax} for the most of the spectrum with the heavier wall (γ=5) being most detrimental. For very stiff frames (T_s<0.6 s), the mass ratio difference has no visible influence on u_{smax}.

Clearly, in some cases (γ≥2000, and T_s>1.5 s), the response of the flexible frame dominates the overall response the RWMF system, and the rotational inertia effect of the rocking wall is negligible. Nevertheless, in some cases (γ≤10 and T_s=0.6 s to 1.4 s), the dynamic of the rocking wall is not negligible and it may be unfavorable because it may drive the structure. The utility of any rocking wall, as part of a building structure, depends upon the relative stiffness of the frame and the rocking wall.

For small mass ratio γ=5 and very flexible frames (T_s>1.5 s), the maximum displacement response is more attenuated in the case of the RWMF system with a squatter wall, tanα=1/2, as shown in Fig. 13 (b).

6. Conclusions

This paper investigates the transient response of a post-tensioned RWMF system. The full nonlinear equations of motions are developed. The model is validated through comparison of the predicted response of the combined system against that obtained from FE analysis when excited by near-fault trigonometric pulse and earthquake-induced ground acceleration. An extensive parametric analysis on the rotation, angular velocity of the rocking wall and the frame displacement leads to the following conclusions:

The RWMF remains a SDOF system throughout the loading history of the structure. The response of the coupled

rocking wall-moment frame system depends on its mass ratio, frame stiffness, wall slenderness, together with the energy loss during impacts.

The forward pulses and forward-and-back pulses with the same amplitude, angular frequency and duration result in different dynamic response of a RWMF system. The trigonometric pulses adopted in this paper illustrate the effects of different types of ground acceleration with excellent clarity.

The rocking wall demonstrates good damping ability for a RWMF system. A restitution coefficient of 0.9 is applied in this paper resorting to experimental information.

The presence of the wall suppresses the maximum displacement response in particular for very flexible frame coupled with a heavier wall. Nevertheless, this effectiveness could vanish for a RWMF system with very stiff frame or affect the response in negative way, resulting in larger displacement for a RWMF system with frames of mild stiffness.

The post-tension cable allows separation to occur between the wall-foundation interfaces, and provides restoring forces for the rocking wall against overturning. The cable is most effective for a RWMF system with very flexible frame.

For a multistory MF coupled with a strong rocking wall, the RWMF system can also be categorized as a SDOF system, since the first mode of vibrations is enforced by allowing the RRW to suppress all higher modes. The concept of base shear effective modal mass and modal height might be adopted in the equivalent SDOF model, as suggested by Chopra (2017).

Acknowledgements

Support for this research was provided by Chinese National Natural Science Foundation (41172267) and National Sci-Tech Support Plan (2015BAB07B05).

References

Ajrab, J.J. (2000), "Rocking wall-frame structures with supplemental damping devices", MS Thesis, University at Buffalo, the State University of New York, Buffalo.

Ajrab, J.J., Pekcan, G. and Mander, J.B. (2004), "Rocking wall-frame structures with supplemental tendon systems", *ASCE J. Struct. Eng.*, **130**(6), 895-903.

Aslam, M., Goddon, W.G. and Scalise, D.T. (1980), "Earthquake rocking response of rigid bodies", *J. Struct. Div.*, ASCE, **106**(2), 377-392.

Barthes, C.B. (2012), "Design of earthquake resistant bridges using rocking columns", Ph.D. Dissertation, University of California, Berkeley.

Chopra, A.K. (2017) *Dynamics of Structures: Theory and Applications to Earthquake Engineering*, 5th Edition, Prentice Hall, Englewood Cliffs, New Jersey,

Costa, A. (2012), "Seismic assessment of the out-of-plane performance of traditional stone masonry walls", Ph.D Dissertation, University of Porto, Porto.

Grigorian, C.E. and Grigorian, M. (2015), "Performance control and efficient design of rocking-wall moment frames", *J. Struct. Eng.*, **142**(2), 04015193.

Housner, G.W. (1963), "The behavior of inverted pendulum structures during earthquakes", *Bull. Seismol. Soc. Am.*, **53**(2), 403-417.

Hu, X. and Zhang, Y. (2012), "Seismic performance of reinforced concrete frames retrofitted with self-centering hybrid wall", *Adv. Struct. Eng.*, **15**(12), 2131-2143.

Loo, W.Y., Quenneville, P. and Chouw, N. (2015), "A low damage and ductile rocking timber wall with passive energy dissipation devices", *Earthq. Struct.*, **9**(1), 127-143.

Makris, N. (2015), "Rigidity-plasticity-viscosity: can electrorheological dampers protect base-isolated structures from near-source ground motions", *Earthq. Eng. Struct. Dyn.*, **26**(5), 571-591.

Makris, N. and Roussos Y. (2000), "Rocking response of rigid blocks under near-source ground motions", *Geotechnique*, **50**(3), 243-262.

Makris, N., and Aghagholizadeh, M. (2017),"The dynamics of an elastic structure coupled with a rocking wall", *Earthquake Engineering and Structural Dynamics*, **46**(6), 945-962.

Makris, N.A. (2014), "Half-century of rocking isolation", *Earthq. Struct.*, **7**(6), 1187-1221.

Prieto, F., Lourenço, P.B. and Oliveira, C. (2004), "Impulsive Dirac-delta forces in the rocking motion", *Earthq. Eng. Struct. Dyn.*, **33**(7), 839-857.

Qu, B., Sanchez-Zamora, F. and Pollino, M. (2014), "Mitigation of inter-story drift concentration in multi-story steel concentrically braced frames through implementation of rocking cores", *Eng. Struct.*, **70**(9), 208-217.

Qu, Z., Wada, A., Motoyui, S., Sakata, H. and Kishiki, S. (2014), "Pin-supported walls for enhancing the seismic performance of building structures", *Earthq. Eng. Struct. Dyn.*, **41**(14), 2075-2091.

Sorrentino, L., AlShawa O.and Decanini L.D. (2011), "The relevance of energy damping in unreinforced masonry rocking mechanisms. Experimental and analytic investigations", *Bull. Earthq. Eng.*, **9**(5), 1617-1642.

Wada, A., Qu, Z., Motoyui, S. and Sakata, H. (2011), "Seismic retrofit of existing SRC frames using rocking walls and steel dampers", *Front. Arch. Civil Eng. China*, **5**(3), 259-266.

Zhang, J. and Makris, N. (2000), "Rocking response of free-standing blocks under cycloidal pulses", *J. Eng. Mech.*, **127**(5), 473-483.

AT